

# High Resolution H I Distributions and Multi-Wavelength Analyses of Magellanic Spirals NGC 4618 and NGC 4625

Jane F. Kaczmarek<sup>1</sup>& Eric M. Wilcots

*University of Wisconsin Madison, Department of Astronomy, 475 N. Charter Street, Madison WI 53706 USA*

jane@astro.wisc.edu, ewilcots@astro.wisc.edu

## ABSTRACT

We present a detailed analysis of high resolution H I observations of the Magellanic spiral galaxies NGC 4618 and NGC 4625. While the H I disk of NGC 4625 is remarkably quiescent with a nearly uniform velocity dispersion and no evidence of H I holes, there is a dynamic interplay between star formation and the distribution of neutral hydrogen in NGC 4618. We calculate the critical density for widespread star formation in each galaxy and find that star formation proceeds even where the surface density of the atomic gas is well below the critical density necessary for global star formation. There are strong spatial correlations in NGC 4618 between UV emission, 1.4 GHz radio continuum emission, and peaks in the H I column density. Despite the apparent overlap of the outer disks of the two galaxies, we find that they are kinematically distinct, indicating that NGC 4618 and NGC 4625 are not interacting. The structure of NGC 4618 and, in particular, the nature of its outer ring, are highly suggestive of an interaction, but the timing and nature of such an interaction remain unclear.

*Subject headings:* galaxies: neutral hydrogen – galaxies: Magellanic spirals – galaxies: individual (NGC 4618 & NGC 4625)

## 1. Introduction

One of the more stunning revelations about the Local Group in the past few years has been the observations of the proper motions of the Magellanic Clouds showing that they are moving at significantly higher velocities than previously thought (e.g. Kallivayalil et al. 2006, Piatek et al. 2008, Besla et al. 2010). One major implication of these results is that the Magellanic Clouds may very well be on their first passage through the Local Group, contradicting the long-held view that they are long-standing companions to the Milky Way. From another point of view, this argument makes sense. The Magellanic Clouds, and the Large Magellanic Cloud in particular, are unlike any

---

<sup>1</sup>Now at Sydney Institute for Astronomy, School of Physics H90, The University of Sydney, NSW 2006, Australia

other companions of the Milky Way, M31, or the vast majority of other spiral galaxies (e.g. James & Ivory 2011). In addition, over the past decade or so we have seen a proliferation of statistically significant samples of galaxies that show that objects sharing the basic morphology of Magellanic spirals are common in both the local Universe and at intermediate redshift (Garland et al. 2004, Ryan-Weber et al. 2003, Sheth et al. 2008). Part of the motivation for the study described here is that the dynamics, structure, and star formation history of the LMC have long been interpreted in the context of its proximity to both the Milky Way and the SMC. The fact that there are so many galaxies that share the LMC’s structure but not its proximity to other massive galaxies, and the possibility that the LMC has only recently entered the Local Group drives us to examine the properties of the larger population of Magellanic spirals in detail sufficient to meaningfully and properly understand how the LMC fits into the larger context of late-type barred galaxies.

The earliest comprehensive look at Magellanic spirals was carried out by de Vaucouleurs & Freeman (1972) who noted the structural similarity between the LMC and a number of other nearby galaxies. Much of the subsequent work was aimed at understanding the origin of the lopsided structure that characterized Magellanic type galaxies. Interactions were primarily believed to be responsible for the asymmetric properties of this class of galaxy; a scenario which was well fit by the LMC itself. Theoretical work and some simulations could also accurately account for the apparent lopsidedness of Magellanic spirals, but not their frequency.

Baldwin et al. (1980) originally suggested that differential precession of the disk in an axisymmetric potential would give rise to the asymmetry characteristic of SBm galaxies. Their proposal, however, predicted that the winding problem would result in the asymmetry dispersing over 5 Gyr, too short a timescale to account for the ubiquity of lopsidedness. Walker, Mihos, & Hernquist (1996) and Zaritsky & Rix (1997) proposed that minor mergers could result in lopsided distributions. Compelling evidence for the role of interactions in accounting for lopsided morphology comes from a statistical survey based on examination of POSS and UK Schmidt plates that found 71/75 Magellanic spirals with well-defined one armed morphologies appear to have a physical neighbor (Odewahn 1994). Wilcots & Prescott (2004), however, showed that only 4 of 13 galaxies from the Odewahn (1994) sample were actually interacting and Wilcots, Lehman & Miller (1996) showed that even those that were interacting did so weakly. These studies weakened the argument that asymmetry is generally caused by interactions, and bolstered a model put forth by Levine and collaborators (Levine & Sparke 1998, Noordermeer, Sparke, & Levine 2001) that lopsidedness is stable once the disk is displaced from the dynamical center of the halo and is allowed to rotate around the center.

One example of an instance in which an interaction may be linked to the characteristics of a Magellanic spiral is the NGC 4618-4625 pair of galaxies. NGC 4618 and NGC 4625 have both been classified as Magellanic-type spirals (Odewahn 1994), though only NGC 4618 exhibits the classic optical morphology of a barred galaxy in this class (de Vaucouleurs & Freeman 1972). Tully (1988) gives a distance of 7.3 Mpc to NGC 4618 and 8.2 Mpc NGC 4625, but their apparently overlapping H I distributions lends support to the notion that interactions play a role in generating

the characteristic morphology (Bush & Wilcots 2004). In addition, recent *GALEX* observations reveal NGC 4625 to have an extended UV disk as well as multiple branching, ragged spiral arms. NGC 4625 has been noted to have one of the largest UV to optical disk (as measured by  $D_{25}$ ) ratios of 4 (Gil de Paz et al. 2005) and an even larger H I to optical disk ratio of 9.8 (Bush & Wilcots 2004). It is remarkably symmetric and Bush & Wilcots (2004) noted that it seems unaffected by its apparent interaction with NGC 4618. From its morphology alone, NGC 4618 appears to be a prototypical Magellanic spiral, with an obvious stellar bar and a lopsided one-armed spiral structure. Both galaxies are host to on-going star formation; in NGC 4618 most of the H I regions lie near the central bar, while in NGC 4625 the star formation is nearly uniformly distributed across its disk.

The goals of this work are to re-examine the issue of whether these two galaxies are indeed interacting and what effect such an interaction may be having on both NGC 4618 and NGC 4625, particularly with regard to star formation. We also seek to better understand the symbiotic relationship between the neutral atomic interstellar medium and star formation in Magellanic spirals. In this paper we present a detailed analysis of high-resolution observations of the neutral gas content of NGC 4618 and NGC 4625, complementing the earlier work of Bush & Wilcots (2004) (hereafter, BW04). We describe our observations in §2 and present the H I distribution and overall kinematics in §3.1. We show the tilted ring models of rotation curves for each galaxy in §3.2. We begin our analysis in §4 by looking at the distribution of massive stars and the structure and kinematics of the neutral gas in each galaxy. §4.1 identifies the H I holes in the center of NGC 4618 and §4.2 looks into correlations with tracers of massive star formation. §4.3 calculates star formation thresholds and the corresponding measured column densities. The velocity dispersion of each H I disk is addressed in §4.4. We discuss the possibility of an ongoing interaction between NGC 4618 and NGC 4625 in §5 and finish our analysis in §6 where we look into the nature of the H I ring around NGC 4618. Our conclusions are stated in §7.

## 2. Observations and Data Reduction

We observed the NGC 4618/4625 system using the Very Large Array in the B and C configurations for total integration times of 36 hours and 20 hours, respectively. After each 50 minute exposure series, a 3 minute observation was taken of the phase calibrator, 1225+368. Two separate observations were made of the amplitude and bandpass calibrator, 1328+307, for 10 minutes each. The AIPS tasks ‘*vlacalib*’ and ‘*vlacal*’ were employed to calibrate both the amplitude and phases, respectively. In order to subtract the continuum and clean our data further, several line-free

---

<sup>0</sup>The National Radio Astronomy Observatory is a facility of the National Science Foundation operated under cooperative agreement by Associated Universities, Inc. This work also made use of observations made with the NASA Galaxy Evolution Explorer. *GALEX* is operated for NASA by the California Institute of Technology under NASA contract NAS5-98034.

channels were fit and then subtracted off using the AIPS task ‘*uvlin*’. The task ‘*imagr*’ was used to create and clean both a naturally weighted (robust 5) and intermediately weighted (robust 0) image cube of the galaxy systems. 1000 clean iterations were done to remove the side lobes from our intermediately weighted cube and 1800 for our naturally weighted cube. Our beam size was  $13.14'' \times 13.02''$  for the naturally weighted and  $10.02'' \times 9.40''$  for the intermediately weighted cubes. We compare this to the resolution of BW04 of  $19.6'' \times 16.9''$ . The angular extent of 1 arcsecond corresponds to 35.4 pc for the distance to NGC 4618 (7.3 Mpc) and 39.7 pc for the distance to NGC 4625 (8.2 Mpc) on the sky. Our cube has a velocity resolution of  $5.2 \text{ km s}^{-1}$  and spans a velocity range of  $255.9 - 850.4 \text{ km s}^{-1}$ . We adopt redshift-independent distances in our analysis of the galaxies in order to avoid any local gravitational effects on the measured distances. From Tully (1988), we use a distance of 7.3 Mpc and 8.2 Mpc to NGC 4618 and NGC 4625, respectively.

### 3. Results

#### 3.1. Distribution and Kinematics of H I

A naturally weighted cube was used to produce Figures 1-5. A flux cut off of  $2\sigma$  ( $0.64 \times 10^{-4} \text{ Jy B}^{-1}$  or  $7.3 \times 10^{-1} \text{ M}_{\odot} \text{pc}^{-2}$ ) was applied to the resulting images: the integrated-flux density (moment 0), the velocity field (moment 1), and the velocity dispersion (moment 2). We also create an intermediately weighted data cube (robust 0) and apply a flux cut off of  $2 \times 10^{-4} \text{ Jy B}^{-1}$  ( $2.3 \times 10^{-1} \text{ M}_{\odot} \text{pc}^{-2}$ ). We do this with the motivation of taking advantage of the higher resolution data available for analysis of the H I holes, star-formation thresholds and investigation of the overall fine structure of the galaxies.

Figure 1 shows the emission of each channel of the naturally weighted cube and Figure 2 shows the integrated-intensity map of NGC 4618 and NGC 4625. NGC 4618 is located at (R.A. =  $12^{\text{h}}41^{\text{m}}35^{\text{s}}$ , dec =  $41^{\circ}08'23''$  [J2000]) corresponding to the southwestern portion of the image and NGC 4625 in the northeast corner is located at (R.A. =  $12^{\text{h}}41^{\text{m}}52^{\text{s}}$ , dec =  $41^{\circ}16'18''$  [J2000]). NGC 4625 first appears in the upper left panel of Figure 1 at a velocity of  $648.8 \text{ km s}^{-1}$  with the initial emission from NGC 4618 appearing at a velocity of  $617.7 \text{ km s}^{-1}$ . NGC 4625 disappears by a velocity of  $560.8 \text{ km s}^{-1}$ . The channel maps reveal the complex extended structure of NGC 4618 which we characterize as a ring. This extended emission is notable as the gas north of the main body of NGC 4618 most readily seen in the channels displayed in the upper right panel of Figure 1. By the end of the cube in the lower left panel of Figure 1, the extended gas is seen largely to the south of the main body of NGC 4618.

The large, extended H I ring surrounding the disk of NGC 4618, as well as a number of holes in the H I distribution in the central regions of the galaxy, are evident in the moment 0 map in Figures 2 and 3. Figure 3 represents the integrated H I map overlaid on the SDSS r-band image of the NGC 4618 & NGC 4625 field. The H I contours and beam size are the same as in Figure 2. We identify and discuss the holes in further detail in §4.1 and the ring in §6. Even at this higher



resolution NGC 4625 seems to lack the H I holes we see in NGC 4618. NGC 4625 also lacks the very high column density peaks we see in NGC 4618. From the integrated H I column densities, we measure average column densities of 9.3 and 3.9  $\text{M}_{\odot}\text{pc}^{-2}$  for the central, optically bright regions of NGC 4618 and NGC 4625, respectively. An average density of 0.9  $\text{M}_{\odot}\text{pc}^{-2}$  is measured in the ring of NGC 4618 and 3.02  $\text{M}_{\odot}\text{pc}^{-2}$  in the brightest star-forming arm of NGC 4625 as identified in Figure 3.

Figure 4 shows the velocity field of both galaxies. NGC 4625 shows little evidence of any perturbation or deviation from a typical differentially rotating disk, though there may be evidence of streaming caused by the spiral arm in the southwest corner of the galaxy as indicated by kinks in the isovelocity contours associated with the spiral arms. The velocity field of NGC 4618, however, is quite different. The velocity field of the gas that is spatially coincident with the main stellar body shows a severe twist, consistent with the “S” shaped isovelocity contours one expects to see in a barred galaxy (Kalnajs 1978). As BW04 showed, the outer ring of the galaxy appears to be a separate kinematical component and not necessarily a smooth extension of the inner disk. We discuss the origin and nature of the H I ring later in §6.

Finally, we show the velocity dispersion maps of each galaxy in Figure 5. Once again, NGC 4625 appears to have a quiescent disk with nearly constant velocity dispersion across its full extent. We see the velocity dispersion in both NGC 4618 and NGC 4625 peak in those same regions where the H I column density is highest. The ring around NGC 4618 is also kinematically cold with an average velocity dispersion of  $\sim 10 \text{ km s}^{-1}$ . The most interesting feature in Figure 5 is the very high values in the region where the disks of the two galaxies appear to overlap. We discuss in §5 that this is simply a reflection of the fact that the disks are kinematically distinct.

### 3.2. Rotation Curves

To analyze the nature of the kinematics in both galaxies in more detail we attempted to fit tilted ring models to the velocity fields in Figure 4 using the AIPS task ‘*gal*’. In our model of NGC 4618, the disk and ring of the galaxy are fit separately in order to accurately map the entire observed extent of the galaxy. Attempts to fit the galaxy as a continuous body resulted in nonsensical curves, likely due to the large gap between the disk and the H I ring. Throughout, we allow the inclination and position angle to vary while keeping the center and systemic velocity fixed. The position angle of the major axis and the inclination of the disk are plotted with along with the rotation curves of the corresponding section of the galaxy in Figure 6.

Our fit to the velocity field of NGC 4618 shows that the position angle is nearly constant through the inner part of NGC 4618 out to a radius of 55″. The sharp change in the inclination and rotational velocity at 50 - 55″ indicate the extent of the stellar bar in the center of the galaxy. Beyond a radius of 55″ the position angle smoothly changes by  $\sim 50^{\circ}$  over 80″. The inclination smoothly decreases from  $80^{\circ}$  to just below  $30^{\circ}$  over the inner 60″ and remains relatively constant

beyond that.

To best represent NGC 4625, we average six different solutions of the task ‘*gal*’, simultaneously plotted below the final solution in Figure 7. For each solution, the only variation between the input parameters was slightly different position angles or inclinations, each leading to a unique solution. The spiral arms of NGC 4625 are located at a radius of 80 arcseconds which we see corresponds to the peaks in the inclination, so it is likely that this feature is a result of streaming motions along the arms.

In both models of the galaxies, we see rotational velocities consistent with other Magellanic and late-type spirals. Our results are in agreement with those shown in BW04 and are comparable to van Moorsel’s (1983) previous work on NGC 4618 and NGC 4625. Our differences likely stem from our better resolution. Our range of inclination in the disk of NGC 4618 agree well with those in BW04; however, we derive a narrower range of inclination values for the outer ring which varies from  $30^\circ - 45^\circ$  and has a trend of increasing inclination with increasing radius. Our results for NGC 4625 also agree well with the previous rotation curves from BW04, with our inclination having a smaller range than that of BW04 where the fitted inclination varied between  $20^\circ$  and  $40^\circ$  whereas our results span angles of  $24^\circ$  to  $36^\circ$ .

#### 4. Massive Stars and the Interstellar Medium in NGC 4618 and NGC 4625

Much of the motivation for this work was to better understand the symbiotic relationship between massive stars and the distribution and kinematics of the neutral interstellar medium in both galaxies. We approach this problem by looking at the properties of H I holes in both galaxies and by correlating observational tracers of massive star formation with the distribution and kinematics of the H I. As nicely summarized by Bagetakos et al. (2011), the issue of how feedback from massive stars influences the interstellar medium has been studied extensively for quite some time. In the standard analysis, perhaps best described by McCray & Kafatos (1987) and Tenorio-Tagle et al. (2005), H I holes are the result of feedback from the evolution of massive stars where powerful supernovae eventually clear out areas in the interstellar medium, creating a hot bubble that will expand until the velocity of the gas slows to that of the velocity dispersion of the galaxy. This model has formed the basis of the interpretation of a number of studies of the distribution and properties of H I holes in nearby galaxies (e.g. Puche et al. 1992, Wilcots & Miller 1998). More recent analyses (e.g. Silich et al. 2006, Warren et al. 2011, Weisz et al. 2009, Cannon et al. 2011) suggest a more complex process, which involves multiple generations of star formation. In an analysis of H I holes in galaxies in the THINGS survey Bagetakos et al. (2011) conclude that holes are ultimately the result of feedback from star formation.

In either scenario, the gas removed by the supernova bubble can pile up in areas surrounding the gas-deficient holes where the resulting increase in density can lead to positive feedback in the form of increased star formation. In principle; one might therefore expect the H I holes to be

expanding, contain a concentration of young stars and be surrounded by ongoing star formation. A detailed examination of the stellar content within the holes is beyond the scope of this paper.

To further probe the nature of the star formation and feedback in both galaxies we constructed maps of the 1.4 GHz radio continuum emission associated with NGC 4618 and NGC 4625 by combining all the line-free channels of our intermediate data cube to create a composite image. The 1.4 GHz radio continuum traces both the thermal (free-free) and non-thermal (synchrotron) emission associated with massive star formation (Condon 1992). The former is directly correlated with H II regions while the synchrotron emission is associated with supernovae explosions (e.g. Chomiuk & Wilcots 2009). In either case the 1.4 GHz radio continuum is an excellent tracer of massive stars. Having only a single frequency to work with we cannot accurately separate the two components, however Heesen et al (2011) find that 50% of the 1.4 GHz emission in the irregular galaxy IC 10 is thermal while Kepley et al. (2011) found that up to 40% of the 1.4 GHz emission in NGC 4214 is thermal. For our analyses, we take 50% of our continuum emission to be thermal.

#### 4.1. Identification of H I Holes

H I holes in the disk of NGC 4618 were first noted in BW04. Utilizing our new high resolution column density and velocity maps we identify six distinct holes in NGC 4618. The positions of the holes are listed in Table 1 and shown in Figure 8. All holes are defined as coherent structures having a H I surface density less than  $6.42 \text{ M}_{\odot} \text{pc}^{-2}$ .

Table 1: Properties of H I Holes

Classified Hole Number	Center RA	Center Dec
1	$12^h 41^m 30.9^s$	$41^{\circ} 07' 45'' .8$
2	$12^h 41^m 32.8^s$	$41^{\circ} 07' 54'' .4$
3	$12^h 41^m 35.5^s$	$41^{\circ} 08' 50'' .3$
4	$12^h 41^m 35.4^s$	$41^{\circ} 10' 07'' .6$
5	$12^h 41^m 32.4^s$	$41^{\circ} 09' 16'' .0$
6	$12^h 41^m 32.4^s$	$41^{\circ} 08' 50'' .2$

To better understand the physical nature of the holes we examined the kinematics of the H I surrounding each one. The velocity profiles were plotted using the AIPS task *plcub* where each box represents the H I profile (intensity vs. velocity) for a region equivalent to  $\sim 250 \text{ pc}$  on a side in the galaxy (Figure 9). The general absence of double peaked and broad profiles of the surrounding gas makes is a compelling argument that the H I holes are not expanding. More significantly, there is essentially no velocity gradient across the hole as one would expect if the holes were expanding. Therefore, if the holes were caused by stellar feedback, the events occurred long enough ago that the expansion has stopped. Without a detailed analysis of the underlying stellar population we cannot put a constraint on the timescale of such an event.

#### 4.2. Correlations with UV and 1.4 GHz Emission

Even in the absence of analysis of the stellar population we can correlate the position of the H I holes with recent star formation as traced by its UV emission as seen by *GALEX*. In Figure 10 we plot the NUV emission from *GALEX* with red contours, the H I column density in blue, and the 1.4 GHz continuum emission (discussed in more detail below) in green. Each is overplotted on an image of NGC 4618 taken from a r-band Sloan Digital Sky Survey DR7 (Abazajian et al. 2009). The most obvious feature is the apparent stellar bar in which we seen copious UV emission (red contours) and enhanced 1.4 GHz emission. There is an overall deficit of H I in the bar, similar to the lack of H I seen in the stellar bar of the LMC (Staveley-Smith et al. 2003). While there is a significant concentration of UV and 1.4 GHz emission associated with the bar in NGC 4618, we also see an enhancement in the UV emission along the rim of the large complex of H I holes 1 & 2 (Figure 8) in the southern half of the galaxy. The local peak of the UV emission in the arm ( $12^h41^m33^s$ ,  $+41^\circ08'30''$ ) is also coincident with a ridge of 1.4 GHz emission and an enhancement in the underlying distribution of stars. This type of phenomenology is what one would expect if the expansion of the hole leads to an enhancement in the ISM density and subsequent star formation along a shell surrounding the hole. Additional peaks in UV emission are in close proximity to, but slightly offset from, corresponding peaks in the H I column density along the arm.

The brightest peak in UV emission ( $12^h41^m31.7^s$   $+41^\circ08'0.5''$ ) in NGC 4618 has a flux comparable to that of a massive star cluster and is located on a wispy H I filament with a density of  $7.3 \text{ M}_\odot \text{pc}^{-2}$ . This ridge of H I can most easily be seen in Figure 8 separating holes 1 & 2. We analyzed the *GALEX* observations and derived FUV and NUV fluxes of  $1477 \mu\text{Jy}$  and  $970 \mu\text{Jy}$ , respectively, equivalent to  $1.9 \times 10^{-14}$  and  $5.5 \times 10^{-15} \text{ erg s}^{-1} \text{ cm}^{-2} \text{ \AA}^{-1}$  ( $-14.30$  and  $-12.95$  magnitudes, respectively). These fluxes are a few times lower than the  $9.8 \times 10^{-14} \text{ erg s}^{-1} \text{ cm}^{-2} \text{ \AA}^{-1}$  measured in NGC 5471, a giant H II region in M101 (Garcia-Benito et al. 2011). We conclude that this source is likely a giant star cluster in NGC 4618 and may have been responsible for the formation of H I holes in the southern part of the galaxy.

In the disk of NGC 4625, we see no radio continuum emission, but observe prominent UV emission arising from the areas of highest H I column density (e.g. the disk and brightest spiral arm) as shown in Figure 11. Gil de Paz et al (2005) studied the UV emission in the disk of NGC 4625 in great detail and suggest the possible existence of multiple spiral arms and large structures associated with the galaxy. They also point out that the UV emission extends roughly four times farther than the stellar disk as measured by  $D_{25}$  (Figure 3 of Gil de Paz et al. 2005). Gil de Paz et al (2005) reason that the UV emission at the large radii is likely due to gravitational instability in the outer H I disk. They further suggest the likelihood of an unknown additional factor that is affecting only the disk of NGC 4625 in order to account for the lack of extended UV emission in NGC 4618. If the extended UV emission is indeed due to a gravitational instability in the disk, it would have to be caused by an current interaction with NGC 4625A, due to the lack of an interaction between NGC 4618 and NGC 4625, as we argue in §5. It is difficult, however, to say to what degree the proposed dwarf galaxy could perterb the disk of the significantly more massive

NGC 4625. What we see in Figure 11 is that the H I disk of NGC 4625 is quite extended and that the UV emission falls along enhancements in the H I column density that morphologically resemble spiral arms. Gil de Paz et al. (2005) suggest that there is faint UV emission associated with what we now see as the outermost H I arm.

### 4.3. Star Formation Thresholds and H I Column Densities

Kennicutt (1989) argued that large scale star formation in disk galaxies only occurs once the surface density of gas crosses a certain threshold following the global definition of the critical density,

$$\Sigma_c = \alpha \frac{\kappa c}{3.36G}$$

where  $\kappa$  is the epicyclic frequency,

$$\kappa = 1.41 \frac{V}{R} \left(1 + \frac{R}{V} \frac{dV}{dR}\right)^{1/2}$$

$c$  is the velocity dispersion and  $\alpha$  is a dimensionless constant often taken to be less than 1 due to the existence of fluid instabilities in a gas and stellar disk (Jog & Solomon 1984*a,b*). While it is clear that the more accurate assessment of the critical density requires knowledge of the molecular content (e.g. Schrubba et al. 2011), we can compare the surface density of atomic gas and the critical density with our existing data. We adopt a value for  $\alpha=0.67$ , which is the mean value for a sample of disk galaxies as derived by Kennicutt (1989). The value for the velocity dispersion of the gas,  $c$ , was taken to be the measured average value from the respective regions on our velocity dispersion map (Figure 5).

Using the above mentioned values and those listed in Table 2, we calculate the star formation threshold for the distinct areas in each galaxy. For NGC 4618, the disk has a calculated critical density of  $40 \text{ M}_\odot \text{pc}^{-2}$ , whereas the ring has a much lower threshold at  $6.5 \text{ M}_\odot \text{pc}^{-2}$ . This large difference is the result of the steep rise in the rotation curve in the central parts of the galaxy while the rotation curve in the outer ring is flat. The threshold in the center of NGC 4625 is  $39 \text{ M}_\odot \text{pc}^{-2}$  and  $\sim 11 \text{ M}_\odot \text{pc}^{-2}$  in the spiral arm.

With the motivation of understanding the global star formation thresholds in both galaxies, we derive corresponding H I column densities for the distinct areas in both galaxies, using beam size and average flux per beam as stated in §2. The observed peak surface density in the disk of NGC 4618 (Figure 10) is  $\sim 21 \text{ M}_\odot \text{pc}^{-2}$ , a factor of two below the nominal critical density. The ring surrounding NGC 4618, which is not seen to have on-going star formation, is measured at having an average density of  $0.9 \text{ M}_\odot \text{pc}^{-2}$ , well below the calculated critical density.

Table 2: Values for Critical Density Calculations

Galaxy	Region	Radius	Velocity	c	$\frac{dV}{dR}$	$\Sigma_c$
		(kpc)	(km s <sup>-1</sup> )	(km s <sup>-1</sup> )	( $\frac{km}{s \ pc}$ )	(M <sub>⊙</sub> pc <sup>-2</sup> )
NGC 4618	Disk	2.15	80	15.3	.0477	39.97
NGC 4618	Ring	5.82	100	7.0	0	6.47
NGC 4625	Disk	1.42	55	10.0	.0423	39.18
NGC 4625	Stellar Arm	2.65	55	7.3	0	10.79

The surface density of the atomic gas coincident with the optical disk of NGC 4625 is 3.9 M<sub>⊙</sub>pc<sup>-2</sup>, falling to  $\sim 3.0$  M<sub>⊙</sub>pc<sup>-2</sup> for a prominent spiral arm of NGC 4625, as seen in Figure 11. The full radial plots of the H I surface density for both galaxies are shown in Figure 12. These profiles are consistent with the set of radial profiles for another sample of dwarf and irregular galaxies discussed by Wilcots & Hunter (2002).

Gil de Paz et al. (2005) note the existence of the extended UV disk in NGC 4625 and sketch the spiral UV morphology of the disk. The measured H I column density in the outer arms is well below the nominal critical density, however the spiral arms correspond to regions in the disk where the H I peaks and where we observe UV emission and therefore, on-going star formation. In NGC 4625, on-going star formation can be observed to a distance  $\frac{3}{4}$  the radius of the H I disk (BW04), which is also a distance 3 times greater than the radius of the optical disk. The fact is that in both galaxies star formation proceeds even when the surface gas density of the atomic gas is below the nominal critical density. However, we do not include molecular gas and Schrubba et al. (2011), among others, have clearly demonstrated that the surface density of star formation is not well correlated with the surface density of atomic gas in disk galaxies. Our results also reinforce the idea that in many galaxies, the onset of star formation is a result of local events rather than a global instability in the disk.

#### 4.4. Velocity Dispersions of the Disks

The mechanical energy deposited by massive stars into their environment is typically more than sufficient to account for the formation of H I holes, especially when integrated over several generations of stars (e.g. Warren et al. 2011). Thurow & Wilcots (2005) and Wilcots & Thurow (2001) also showed that there is more than enough energy to account for flows of ionized gas in irregular galaxies. The mechanical energy from feedback could also go into heating the cool ISM, resulting in higher H I velocity dispersions around regions of recent star formation. Such correlations are common in star-forming galaxies (e.g. IC 10 [Wilcots & Miller 1998], NGC 1569 [Muehle et al. 2005, Walter et al. 2008]).

The H I velocity dispersion in NGC 4625 is nearly uniform across the entire disk at a value of

$\sim 10 \text{ km s}^{-1}$  with little variation between regions with and without UV emission. Combined with the lack of noticeable H I holes, this suggests that the current and recent star formation in NGC 4625 is having little or no impact on the neutral ISM in the galaxy.

The situation in NGC 4618 is quite different. Not only do we see H I holes, we also see a significant increase in the velocity dispersion of the gas in central regions coincident with the current star formation. We see a peak velocity dispersion of  $30 \text{ km s}^{-1}$  located between the peak in the UV emissions (which we discussed in §4.2) and a star-forming region in the stellar arm. The variation in the velocity dispersion throughout the disk is largely coincident with peaks in the H I column density and ongoing star formation. There are also areas of higher velocity dispersion in the SE and NW corners of the disk where it appears that the disk intersects with the H I ring discussed below. In these regions, the H I profiles are noticeably wider when compared to other sections of the ring.

## 5. Are NGC 4618 and NGC 4625 Interacting?

The notion that NGC 4618 and NGC 4625 are interacting is conveniently consistent with the idea that the asymmetric nature of Magellanic spirals is the result of an interaction with a close neighbor (e.g. Odewahn 1994). The apparent proximity of the galaxies to one another and the apparent overlapping H I distributions are highly suggestive of an interaction. BW04 stated that any interaction between NGC 4618 and NGC 4625 would only be affecting the outermost H I of the galaxies – this led them to believe that the observed asymmetry in the stellar disk of NGC 4618 is not a consequence of the current interaction unless the response of the disks is abnormally rapid. The lack of perturbations seen in the velocity field of NGC 4625 is further indication against any on-going interaction between the two galaxies. In lieu of an on-going interaction, the extended UV emission observed in NGC 4625 cannot be due to gravitational instabilities, as suggested by Gil de Paz et al. (2005). The H I profile asymmetries measured in NGC 4618/4625 are on the order of the asymmetries measured in noninteracting Magellanic spirals (Wilcots & Prescott 2004).

Investigating the H I profiles associated with the region where the galaxies’ H I disks seem to overlap reveals two distinct kinematic components, separated by as much as  $50 \text{ km s}^{-1}$  (Figure 13). If the galaxies were interacting we would expect to see a smooth gradient in the velocity of the gas “bridge.” However, we do not see this, thus the galaxies are likely separated and are not interacting. The lack of broadened profiles or double peaks is further evidence against mixing of the outer disks of the galaxies.

The true separation between the two galaxies is difficult to measure due to the uncertainty in the orientations of the two galaxies relative to each other and the lack of distance indicators that are independent of the local gravity field. However, applying the Tully-Fisher relation, Tully (1988) derived distances of 7.3 and 8.2 Mpc for NGC 4618 and NGC 4625, respectively. The claim that there is a 0.9 Mpc separation between the redshift-independent distances is consistent with

our conclusion that the apparently overlapping H I disks are actually kinematically distinct and the NGC 4618 and NGC 4625 are not currently interacting.

## 6. The Nature of the Ring around NGC 4618

The presence of the H I ring around NGC 4618 is a bit of a mystery. Galaxies with extended H I gas have been known to have H I “streamers” stemming from the disk of the galaxy and wrap around the galaxy either completely or in part (Hunter et al. 1998; van der Hulst 1979; Thomasson & Donner 1993; Noguchi 1988). These streamers are often the consequence of an external perturbation, particularly an interaction with a dwarf companion or massive gas cloud (e.g. Athanassoula & Bosma 1985). It is possible that NGC 4618 does indeed have streamers that are feeding the ring, but at our inclination angle we are observing them face-on. Perhaps NGC 4618 was once like NGC 4449 (Hunter et al 1998), but has long been able to evolve a stable, complete ring, assuming the interaction causing the formation of the ring was not recent.

An investigation into the overall kinematics and timescales of the H I ring surrounding the disk of NGC 4618 gives us some idea of a minimum age of the ring and when NGC 4618 had a previous interaction. For simplicity’s sake, we assume that the H I ring around NGC 4618 is circular; therefore, we measure from our rotation curves a  $v_{circ}$  of  $95 \text{ km s}^{-1}$ , which is the average rotational velocity of the ring. Calculating the orbital speed out to 8.5 kpc, we calculate an orbital period of 456 Myr. The average velocity dispersion across the ring is  $6.8 \text{ km s}^{-1}$ , which translates into an expected width of  $\sim 5 \text{ kpc}$  after 500 Myr of diffusion, assuming a constant velocity dispersion. The maximum velocity dispersion is  $36 \text{ km s}^{-1}$ , which would lead to a width of 18.4 kpc. The observed width of the ring is  $\sim 3.7 \text{ kpc}$ , suggesting that it is either much younger than an orbital period or is at least 450 Myr old and is stable enough to hold itself together.

If the ring is the result of an interaction, it is not at all clear with which galaxy NGC 4618 could have interacted. Using the difference between their systemic velocities and a 900 kpc separation (Tully 1988) between the two galaxies, the minimum crossing time of NGC 4618 and NGC 4625 is  $1.6 \times 10^{10}$  years, longer than the age of the Universe. In order to assess the possibility that either NGC 4618 or 4625 has had a different recent encounter, we used the Sloan Digital Sky Survey (SDSS) DR7 (Abazajian et al. 2009) to search for nearby objects. The closest neighbor is NGC 4490, a spiral galaxy also known as the Cocoon galaxy, with a  $v_{sys} = 565 \text{ km s}^{-1}$  and an angular separation of  $2.74^\circ$  from NGC 4618. At a distance of 7.8 Mpc (Tully 1988) this corresponds to a projected separation of 375 kpc on the sky. The difference between the systemic velocities of NGC 4618 and 4490 is only  $21 \text{ km s}^{-1}$  which would imply a last encounter  $3.8 \times 10^{10}$  years ago. However, we can say nothing about their tangential motions relative to each other. In order for the two galaxies to have crossed 450 Myr ago, NGC 4618 and NGC 4490 would have to be moving at  $\sim 820 \text{ km s}^{-1}$  relative to one another. While this would be an unusually high relative velocity between two galaxies not in a cluster, it is more reasonable to suggest that the ring has survived for 2-3 orbit times and an encounter occurred 1-1.5 Gyr ago.



The ring does not necessarily have to be a remnant of an earlier interaction with another galaxy of similar mass. As in the case of NGC 4618, the ring around NGC 4449 (Hunter et al. 1998) completely encircles the central part of the galaxy at a position angle offset from that of the inner regions. Hunter et al. (1998) suggest that the morphology of the ring around NGC 4449 is the result of an encounter with a nearby dwarf companion. However, aside from the hint of a dwarf companion to NGC 4625 mentioned in Gil de Paz et al. (2005) we see no such companion near NGC 4618.

At this point too little is known about this putative companion, NGC 4625A to say whether or not it is or could have interacted with either NGC 4625 or NGC 4618. The H I disk of NGC 4625 is remarkably quiescent with a nearly uniform velocity dispersion and if the proposed companion galaxy NGC 4625A exists, it is devoid of neutral gas within our velocity range. Our one channel  $5\sigma$  detection for NGC 4625A is  $1.26 \times 10^4 M_\odot$ . This strongly suggests a lack of neutral gas or, if there is gas present, it is not in our velocity range and therefore not a likely companion of NGC 4625, nor NGC 4618. We cannot rule out the possibility that NGC 4625A is a dwarf elliptical or spheroidal companion to NGC 4625.

We are left with the same issue that has long bedeviled our efforts to understand the origin of the asymmetric morphology of Magellanic-type galaxies. Despite the numerous models that show how one can account for the off-center bars and one-armed spiral, NGC 4618 (and most other Magellanic galaxies) show no sign of a companion. Noordermeer, Sparke, & Levine (2001) suggested that disk galaxies, once knocked off-center remains so as long as the disk is much less massive than that the halo. Those authors do not investigate what could have knocked the disk off-center in the first place. Besla et al. (2012) recently proposed that the Magellanic Stream, and the structure of Magellanic galaxies in general, could be explained with the merger of two dwarf galaxies. The implication for our study would be that NGC 4618 is the product of past merger of two galaxies. There has also been a recent suggestion that the characteristic asymmetric morphology of Magellanic spirals could be the result of a collision with a dark satellite (Bekki 2009). The obvious attraction of this suggestion is that it gets around the problem that most Magellanic spirals do not have companions.

## 7. Conclusions

We presented a detailed analysis of high resolution H I observations of NGC 4618 and NGC 4625. In combination with tracers of recent star formation these high resolution H I data allow us to carry out an investigation of the relationship between massive star formation and the distribution and kinematics of the atomic interstellar medium in both galaxies. While the surface density of the atomic gas remains well below the nominal critical density needed for global star formation (e.g. Kennicutt 1989), we do find a spatial correlation between tracers of current star formation and relative peaks in the H I column density. In NGC 4625 star formation traces faint spiral structure that is also seen in the H I column density. In NGC 4618 star formation is found in much of the

disk.

We also noted a number of H I holes in NGC 4618, but also show that the holes are not expanding, and establish anti-correlation between the location of the H I holes and peaks in UV emission for the galaxy. As with a number of other studies we conclude that the major holes are most likely the result of supernovae. However, we reach this conclusion without an understanding of the molecular content of the holes, but believe that the holes are more likely to contain hot ( $10^6$  K) gas rather than cold gas. The 1.4 GHz radio continuum emission stemming from the center of NGC 4618 suggests that the emission stems from multiple supernovae, strengthening the argument that the holes were created through a series of powerful explosions. We investigate the environments in which we observe active star formation in both galaxies and measure H I column densities in the area of the brightest star formation corresponding to the areas of brightest UV emission.

The H I line profiles associated with the gas believed to be the bridge connecting the two galaxies actually has two well-defined and separate kinematic components. This observation makes a strong case against an on-going interaction between the NGC 4618 and NGC 4625 galaxies, in conjunction with the lack of perturbations to either velocity field or the H I velocity dispersion in NGC 4625.

The persistence of the H I ring around NGC 4618 allows for us to apply a rough interaction timescale of 450 Myr, assuming that the ring has successfully completed one complete rotation around the center of the galaxy. Investigating the area that surrounds the NGC 4618/4625 system, we find that NGC 4490 is projected to be relatively close to the pair, yet serves as an unlikely candidate for having previously interacted with NGC 4618. Thus, the origins of the likely stable H I ring around NGC 4618 are still not well understood.

## 8. Acknowledgements

We thank Cody Gerhartz for helpful conversations and contributions to this paper and acknowledge the support of NSF Grant AST-0708002. We also thank the anonymous referee for helpful comments to improve this paper.

## REFERENCES

- Abazajian, K.N., Adelman-McCarthy, J.K., Agueros, M.A., et al. 2009, *ApJ Suppl*, **182**, 543
- Athanassoula, E., & Bosma, A. 1985, *ARA&A*, **23**, 147
- Bagetakos, I., Brinks, E., Walter, F., de Blok, W. J. G., Usero, A., Leroy, A. K., Rich, J. W. & Kennicutt, R. C. 2011, *EAS*, **52**, 103
- Baldwin, J. E., Lynden-Bell, D. & Sancisi, R. 1980, *MNRAS*, **193**, 313
- Bekki, K. 2009, *MNRAS*, **393**, 60
- Besla, G., Kallivayalil, N., Hernquist, L., van der Marel, R. P., Cox, T. J. & Keres, D. 2010, *ApJ*, **721**, 97
- Besla, G., Kallivayalil, N., Hernquist, L., van der Marel, R. P., Cox, T. J. & Keres, D. 2012, *MNRAS*, *accepted*.
- Bush, S. J. & Wilcots, E. M. 2004, *AJ*, **128**, 2789
- Cannon, J. M., Most, H. P., Skillman, E. D., Weisz, D. R., Cook, D., Dolphin, A. E., Kennicutt, R. C., Lee, J., Seth, A., Walter, F. & Warren, S. R. 2011, *ApJ*, **735**, 36
- Chomiuk, L. & Wilcots, E. M. 2009, *ApJ*, **703**, 370
- Condon, J. J. 1992, *ARA&A*, **30**, 575
- de Vaucouleurs, G., & Freeman, K. C. 1972, *Vistas Astron.*, **14**, 163
- Garcia-Benito, R., Perez, E., Diaz, A. I., Maiz Apellaniz, J. & Cervino, M. 2011, *AJ*, **141**, 126
- Garland, C. A., Pisano, D. J., Williams, J. P., Guzman, R. & Castander, F. J. 2004, *ApJ*, **615**, 689
- Gil de Paz, A., Madore, B. F., Boissier, S., Swaters, R., Popescu, C. C., Tuffs, R. J., Sheith, K., Kennicutt, R. C. Jr., Bianchi, L., Thilker, D., & Martin, D. C. 2005, *ApJ*, **627**, L29
- Heesen, V., Rau, U., Rupen, M.P., Brink, E., & Hunter, D.A. 2011. *ApJL*, **739**, L23
- Hunter, D. A., Wilcots, E. M., van Woerden, H., Gallagher, J. S. & Kohle, S. 1998. *ApJ*, **495**, L47
- James, P. A. & Ivory, C. F. 2011, *MNRAS*, **411**, 495
- Jog, C. J., & Solomon, P. M., 1984a, *ApJ*, **276**, 114
- Jog, C. J., & Solomon, P. M., 1984b, *ApJ*, **276**, 127
- Kallivayalil, N., van der Marel, R. & Alcock, C. 2006, *ASPC*, **357**, 70
- Kalnajis, A. J. 1978, *IAUS*, **77**, 113

- Kennicutt R. C., 1989, *ApJ*, **344**, 685
- Kepley, A. A., Zweibel, E. G., Wilcots, E. M., Johnson, K. E. & Robishaw, T. 2011. *ApJ*, **736**, 139
- Levine, S. E. & Sparke, L. S. 1998, *ApJ*, **496**, 13
- McCray, R. & Kafatos, M. 1987, *ApJ*, **317**, 190
- Muehle, S., Klein, U., Wilcots, E.M. & Huttemeister, S. 2005, *AJ*, **130**, 524
- Noguchi M. 1988, *A&A*, **203**, 259
- Noordermeer, E., Sparke, L. S. & Levine, S. E. 2001, *MNRAS*, **328**, 1064
- Odewahn, S. C. 1994, *A&A*, **107**, 1320
- Piatek, S., Pryor, C. & Olszewski, E. W. 2008 *AJ*, **135**, 1024
- Puche, D., Westpfahl, D., Brinks, E & Roy, J-R. 1992, *AJ*, **103**, 1841
- Ryan-Weber, E. V., Webster, R. L. & Staveley-Smith, L. 2003, *MNRAS*, **343** 1195
- Schruba, A., Leroy, A.K., Walter, F., Bigiel, F., Brinks, E., de Blok, W.J.G., Dumas, G., Kramer, C., Rosolowsky, E., Sandstrom, K., Schuster, K., Usero, A., Weiss, A., & Wiesenmeyer, H. 2011, *AJ*, **142** 37
- Sheth, K., Elmegreen, D. M., Elmegreen, B. G., Capak, P., Abraham, R. G., Athanassoula, E., Ellis, R. S., Mobasher, B., Salvato M., Schinnerer, E., Scoville, N. Z., Spalsbury, L., Strubbe, L., Carollo, M., Rich, M. & West, A. A. 2008 *ApJ*, **675** 1141
- Silich, S., Lozinskaya, T., Moiseev, A., Podorvanuk, N., Rosado, M., Borissova, J. & Valdez-Gutierrez, M. 2006, *A&A*, **448**, 123
- Staveley-Smith, L., Kim, S., Calabretta, M. R., Haynes, R. F. & Kesteven, M. J. 2003, *MNRAS*, **339**, 87
- Tenorio-Tagle, G., Silich, S., Rodriguez-Gonzalez, A. & Munoz-Tunon, C. 2005 *ApJ*, **628**, 13
- Thomasson, M. & Donner, K. J. 1993, *A&A*, **272**, 153
- Thurrow, J.C. & Wilcots, E.M. 2005, *AJ*, **129**, 745
- Tully R. B. 1988, *Nearby Galaxy Catalogue*. Cambridge Univ. Press, Cambridge
- van der Hulst J. M. 1979, *A&A*, **75**, 97
- van Moorsel, G. A. 1983, *A&AS*, **54**, 19
- Walker, I. R., Mihos, J. C., Hernquist, L. 1996 *ApJ*, **462**, 121

- Walter, F., Brinks, E., de Blok, W.J.G., Bigiel, F., Kennicutt, R.C., Thornley, M.D. & Leroy, A.K. 2008, *AJ*, **136**, 2563
- Warren, S. R., Weisz, D. R., Skillman, E. D., Cannon, J. M., Dalcanton, J. J., Dolphin, A. E., Kennicutt, R. C., Koribalski, B., Ott, J., Stilp, A. M., Van Dyk, S. D., Walter, F. & West, A. A. 2011, *ApJ*, **738** 10
- Weisz, D. R., Skillman, E. D., Cannon, J. M., Dolphin, A. E., Kennicutt, R. C., Lee, J & Walter, F. 2009, *ApJ*, **704**, 1538
- Wilcots, E.M., & Hunter, D.A. 2002, *AJ*, **123**, 2449
- Wilcots, E. M. & Miller, B. W. 1998, *AJ*, **116**, 2363
- Wilcots, E. M. & Prescott, M. K. M. 2004. *AJ*, **127**, 1900
- Wilcots, E. M. & Thuroow, J.C. 2001, *ApJ*, **555**, 758
- Wilcots, E. M., Lehman, C. & Miller, B. 1996 *AJ*, **111**, 1575
- Zaritsky, D. & Rix, H. 1997, *ApJ*, **477**, 118

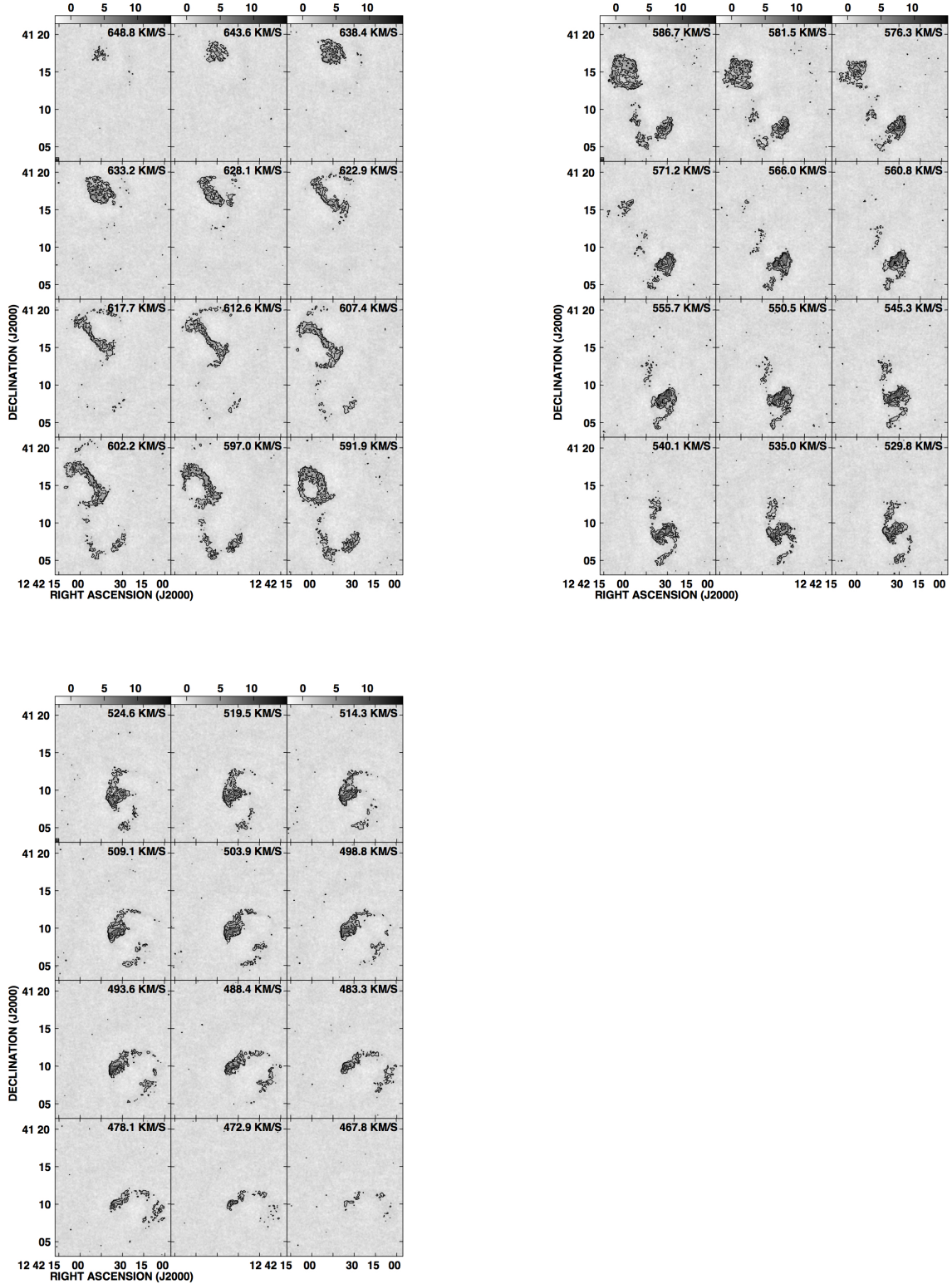


Fig. 1.— Emission in each channel for the naturally weighted data cube. Every channel with signal is shown. The contours are 3, 6 and 12 times the  $2\sigma$  noise level. NGC 4625 first appears in the upper left panel of the top left figure at a velocity of  $648.8 \text{ km s}^{-1}$ , whereas the initial emission from NGC 4618 appears at a velocity of  $617.7 \text{ km s}^{-1}$ . The beam is plotted in the bottom left corner of the top left frame in each image.

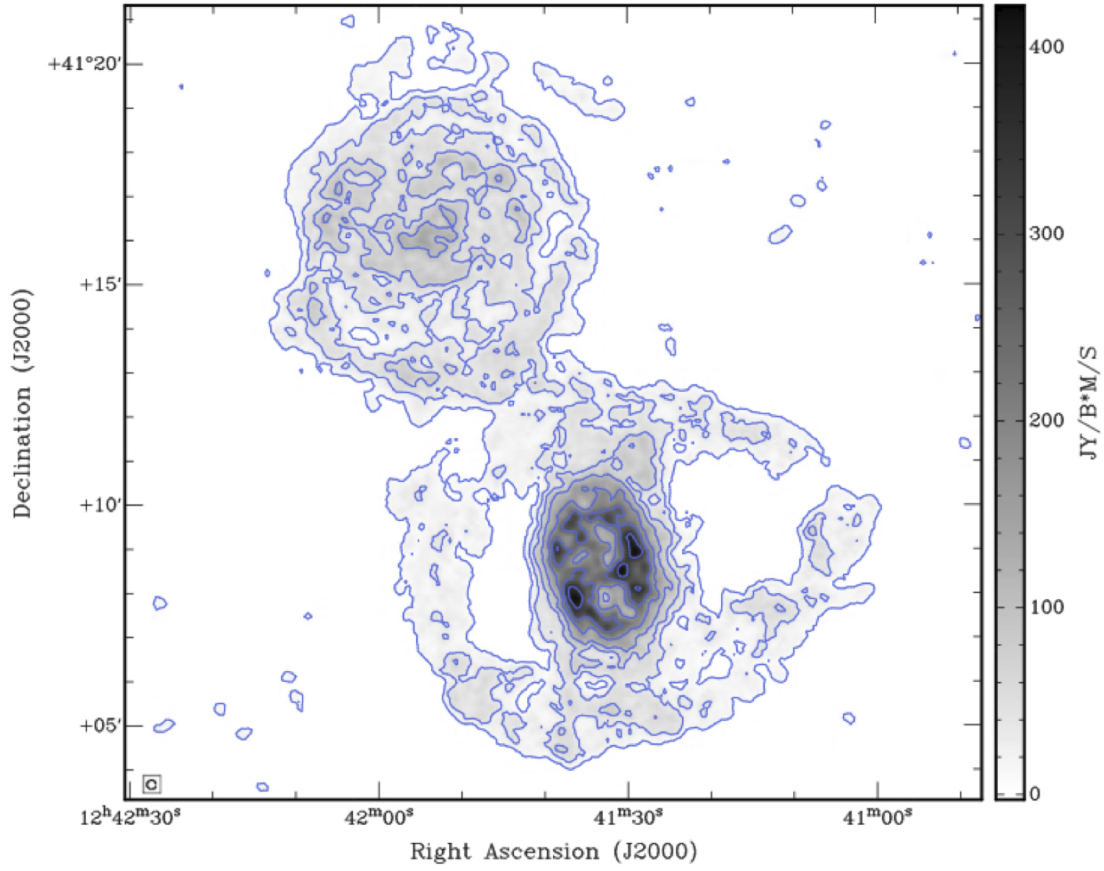


Fig. 2.— Naturally weighted integrated-intensity map of NGC 4618 and NGC 4625. With a peak density of  $21.4 \text{ M}_{\odot} \text{pc}^{-2}$ , the contour lines represent 0.43, 1.7, 3.2, 5.4, 8.5, 12.8 and  $17.1 \text{ M}_{\odot} \text{pc}^{-2}$ . The beam is plotted in the lower left corner for reference. The contrast between the peak column densities in each galaxy stands out. We note the existence a several H I holes in NGC 4618 while none exist in NGC 4625. It is also clear that NGC 4618 is encircled by a substantial ring of H I gas which is discussed in more detail in section 6.

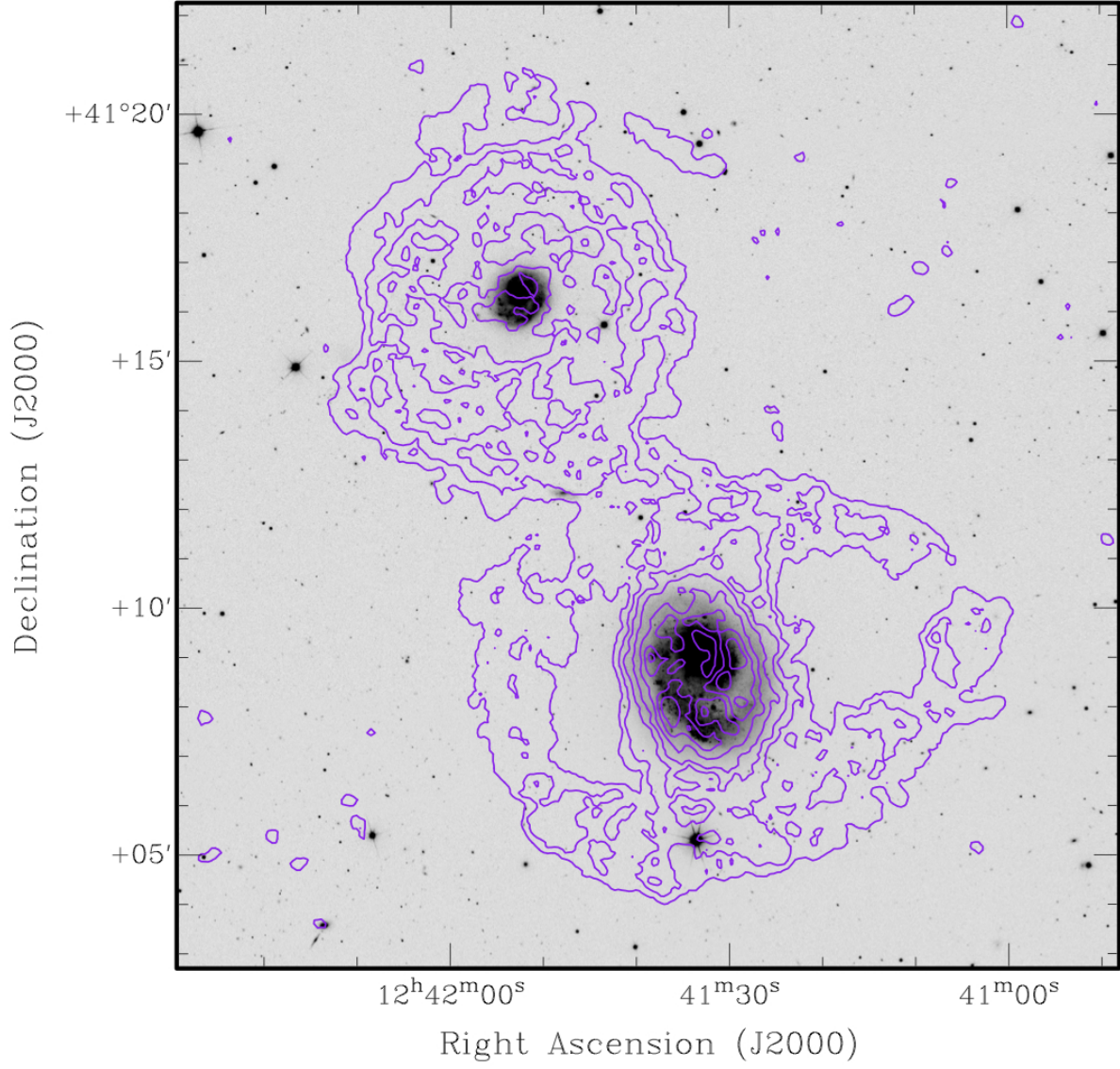


Fig. 3.— Integrated H I map overlaid on the SDSS r-band image of the NGC 4618 & NGC 4625 field. The H I contours represent the same intensity levels as Figure 2. The H I beam is the same as that shown in Figure 2. We note in NGC 4625 the large H I to optical disk ratio of 9.8 (Bush & Wilcots 2004)



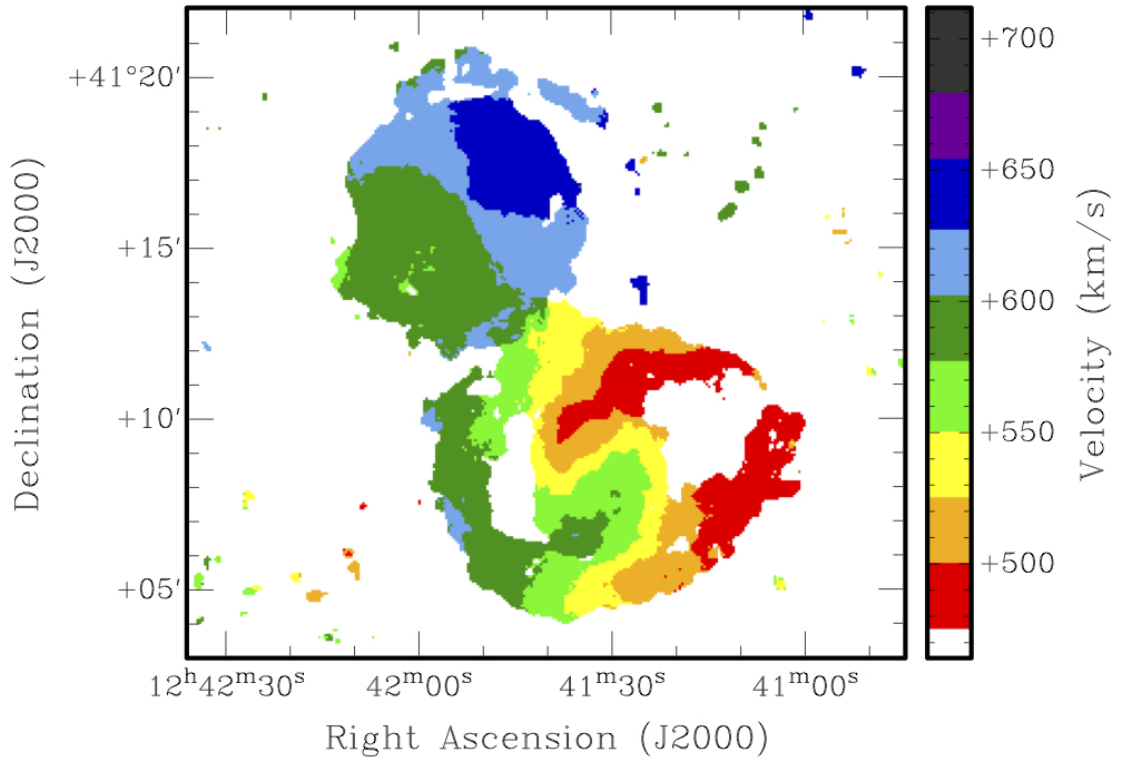


Fig. 4.— Velocity map of naturally weighted data cube of NGC 4618 and NGC 4625. The contours denote a velocity change of  $10 \text{ km s}^{-1}$ . NGC 4625 typifies a differentially rotating disk, whereas NGC 4618 displays an “S” shaped isovelocity curve in the area associated with the stellar bar.

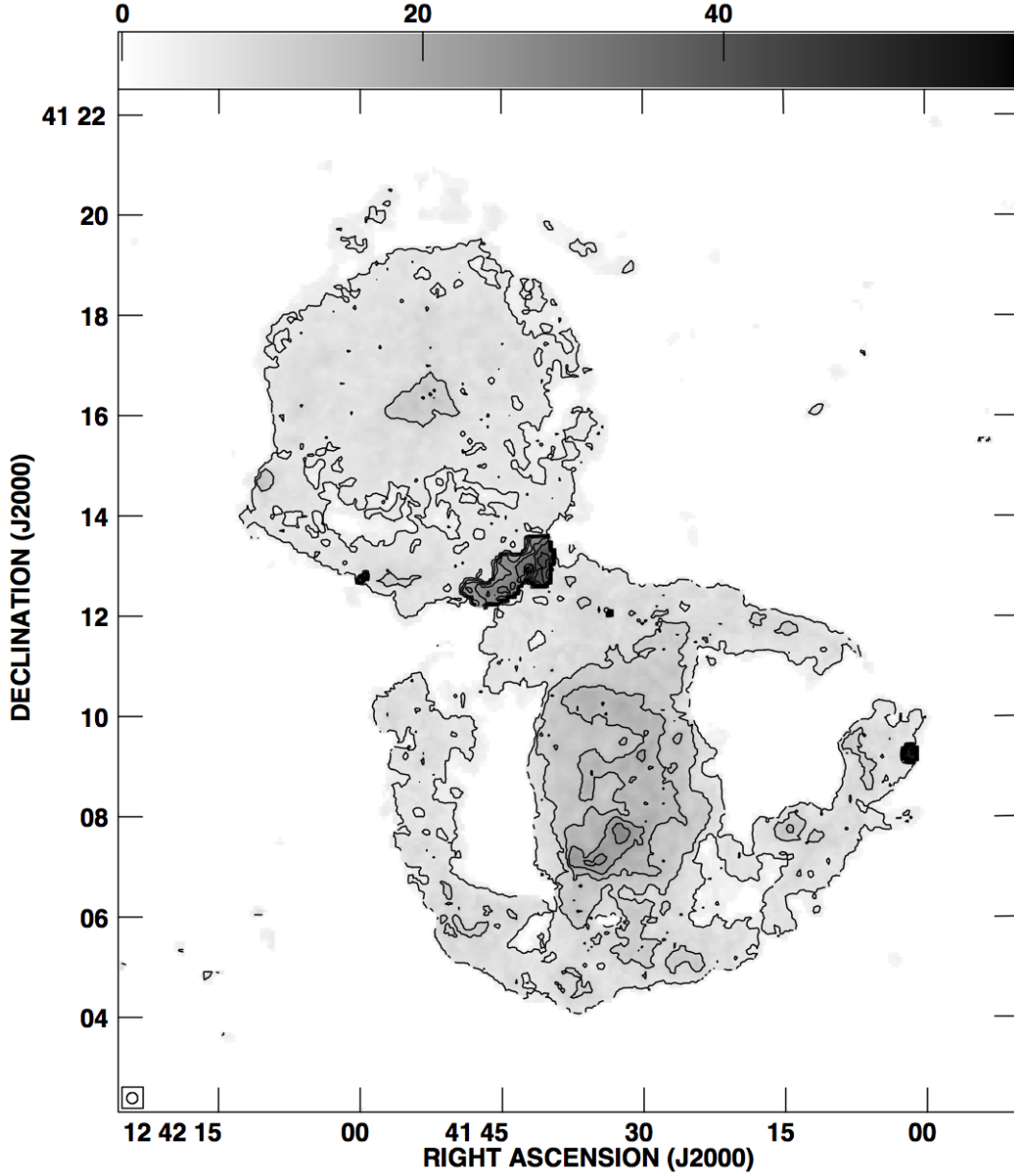


Fig. 5.— Velocity dispersion of naturally weighted data cube of NGC 4618 and NGC 4625. The area of a potential overlap correlates to the area of the largest velocity dispersion. In NGC 4625, we see a remarkably constant velocity across the disk with the exception of the central region. The peaks in velocity dispersion in NGC 4618 are within the stellar extent of the galaxy.

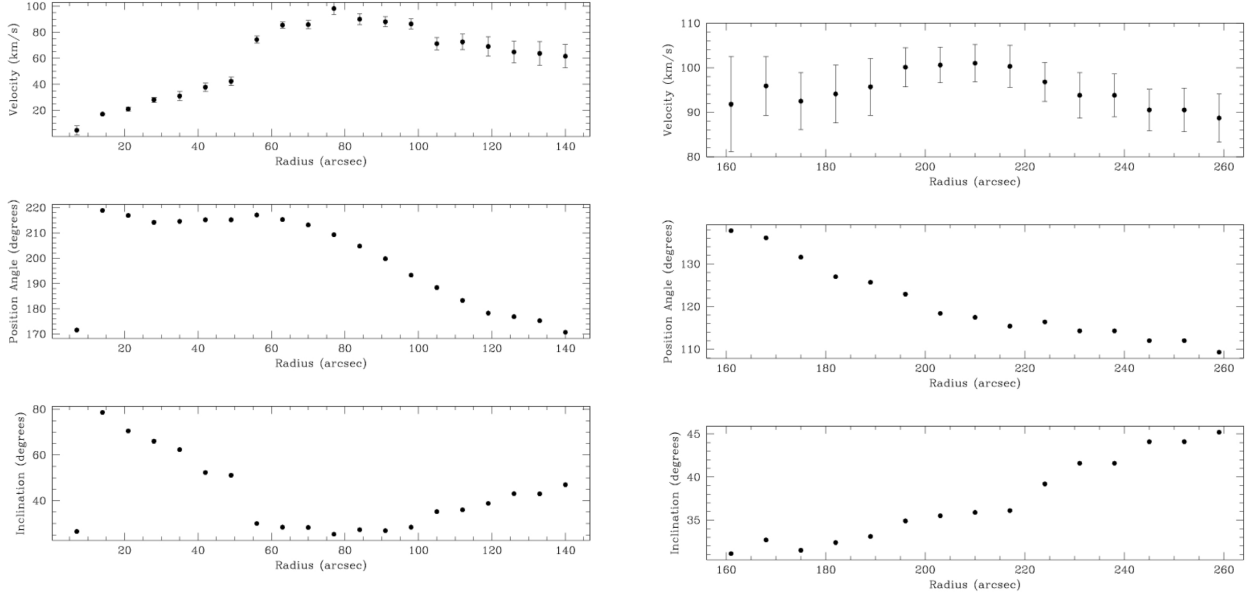


Fig. 6.— Rotation curve, position angle and inclination representing the optical disk (*left*) and the H I ring (*right*) for NGC 4618. We integrate using  $7''$  rings. We note the shallow nature of the inner rotation curve (*top panel*). We can see a large jump from the disk to the ring of the galaxy in both position angle and inclination.

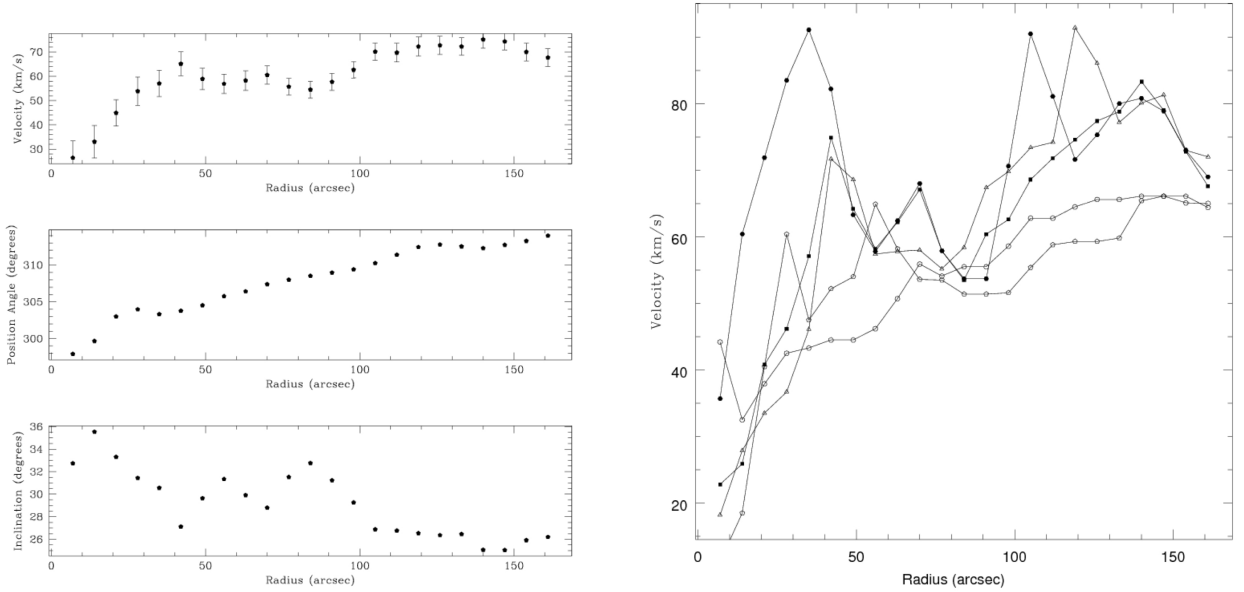


Fig. 7.— (*Top*) Rotation curve, position angle and inclination corresponding to the averaged results from 6 solutions of ‘gal’ for NGC 4625. Just as with NGC 4618, we integrate using  $7''$  rings. (*Bottom*) The six separate solutions to the average rotation curve corresponding to each running of ‘gal’.

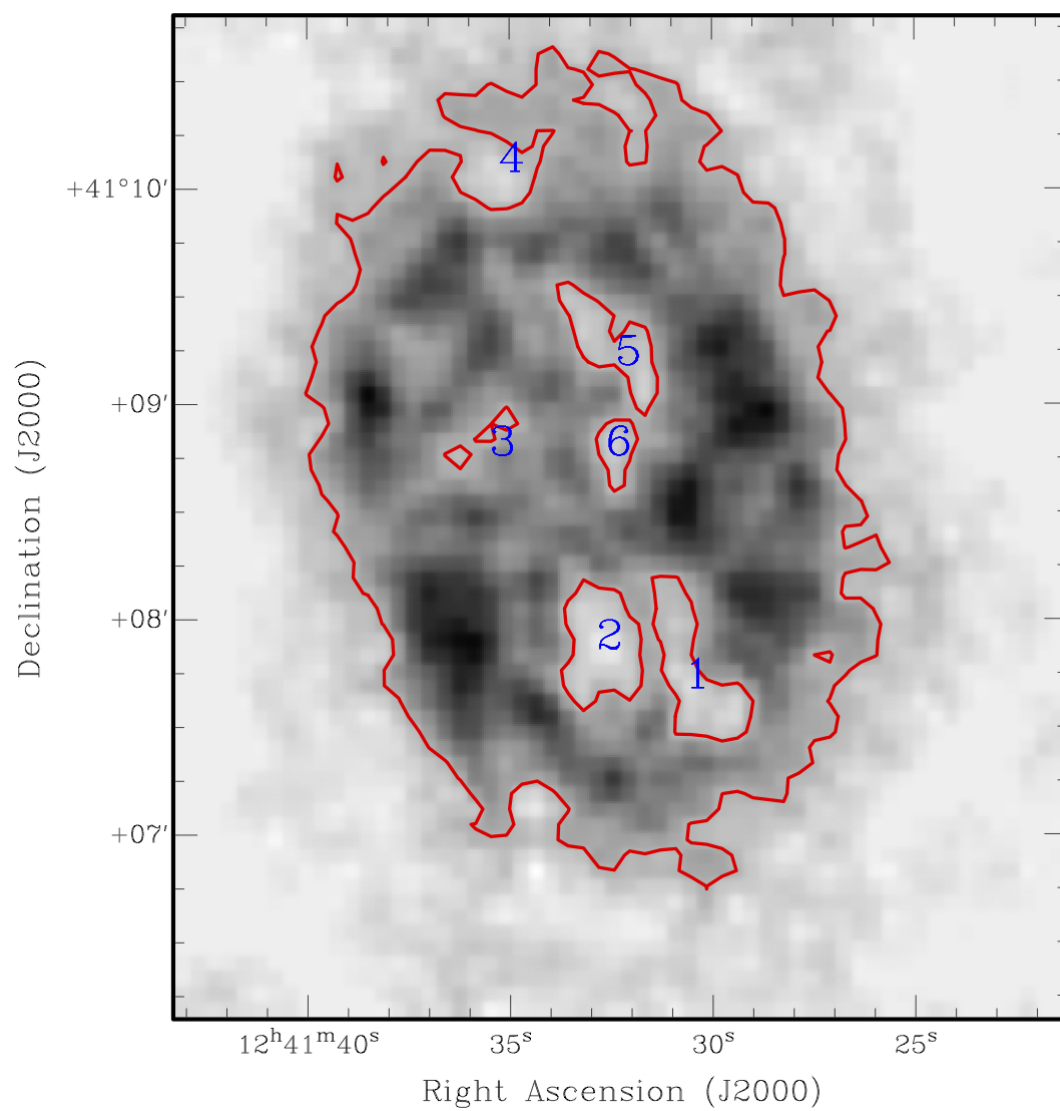


Fig. 8.— Robust 0 moment 1 map with the six H I holes having column densities less than 6.42 M<sub>⊙</sub>pc<sup>-2</sup>. labeled.

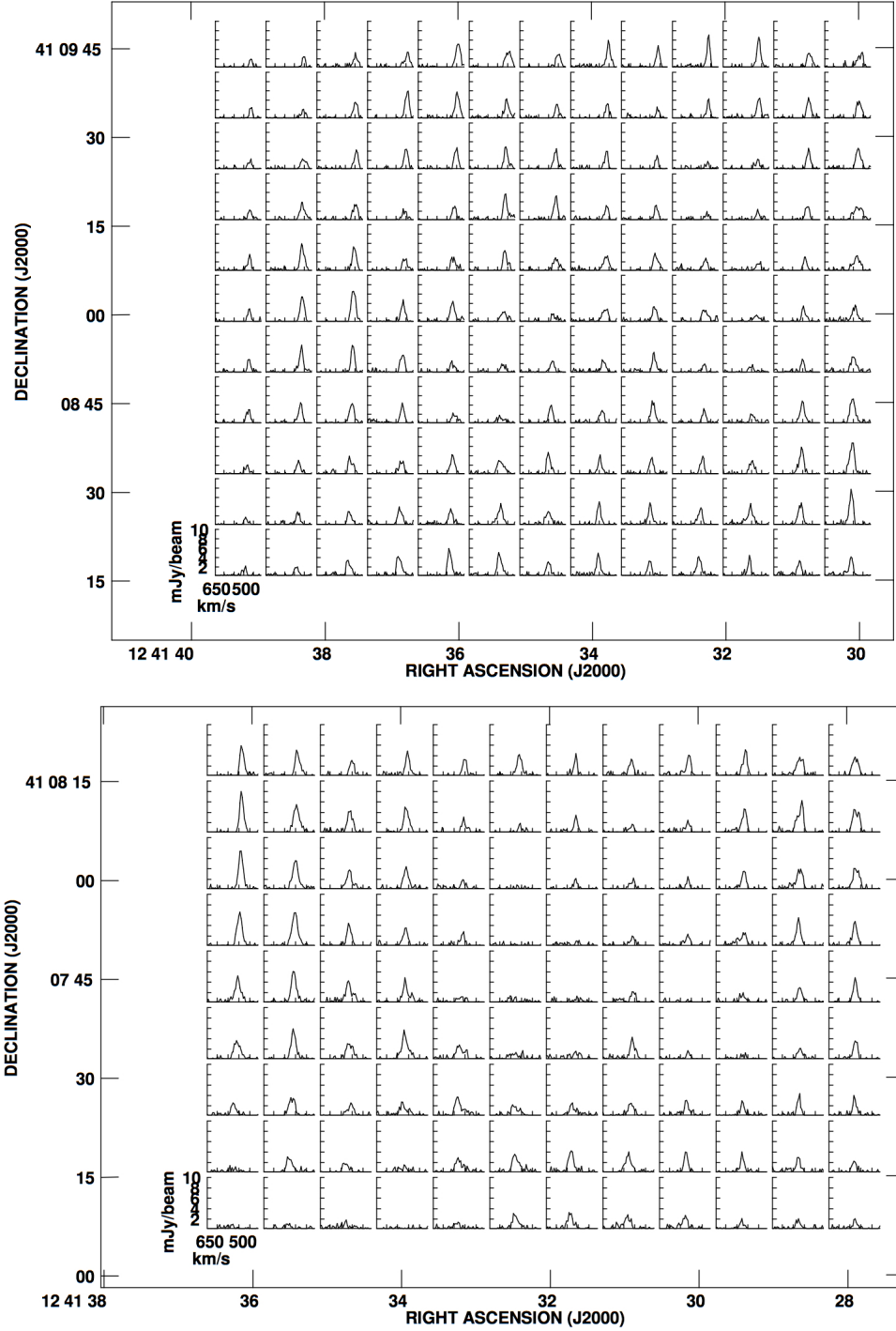


Fig. 9.— The velocity profiles of the region surrounding holes 1, 2 3, 5 and 6, as shown in Figure 8. Each box represents the H I profile for a region equivalent to the beam. A flux cut off of  $2.00 \times 10^{-4} \text{ Jy B}^{-1}$  was applied to the displayed line profiles of the intermediately weighted data cube (Robust 0). The profiles seem devoid of double peaks and significant broadening, arguing against the expansion of the holes.

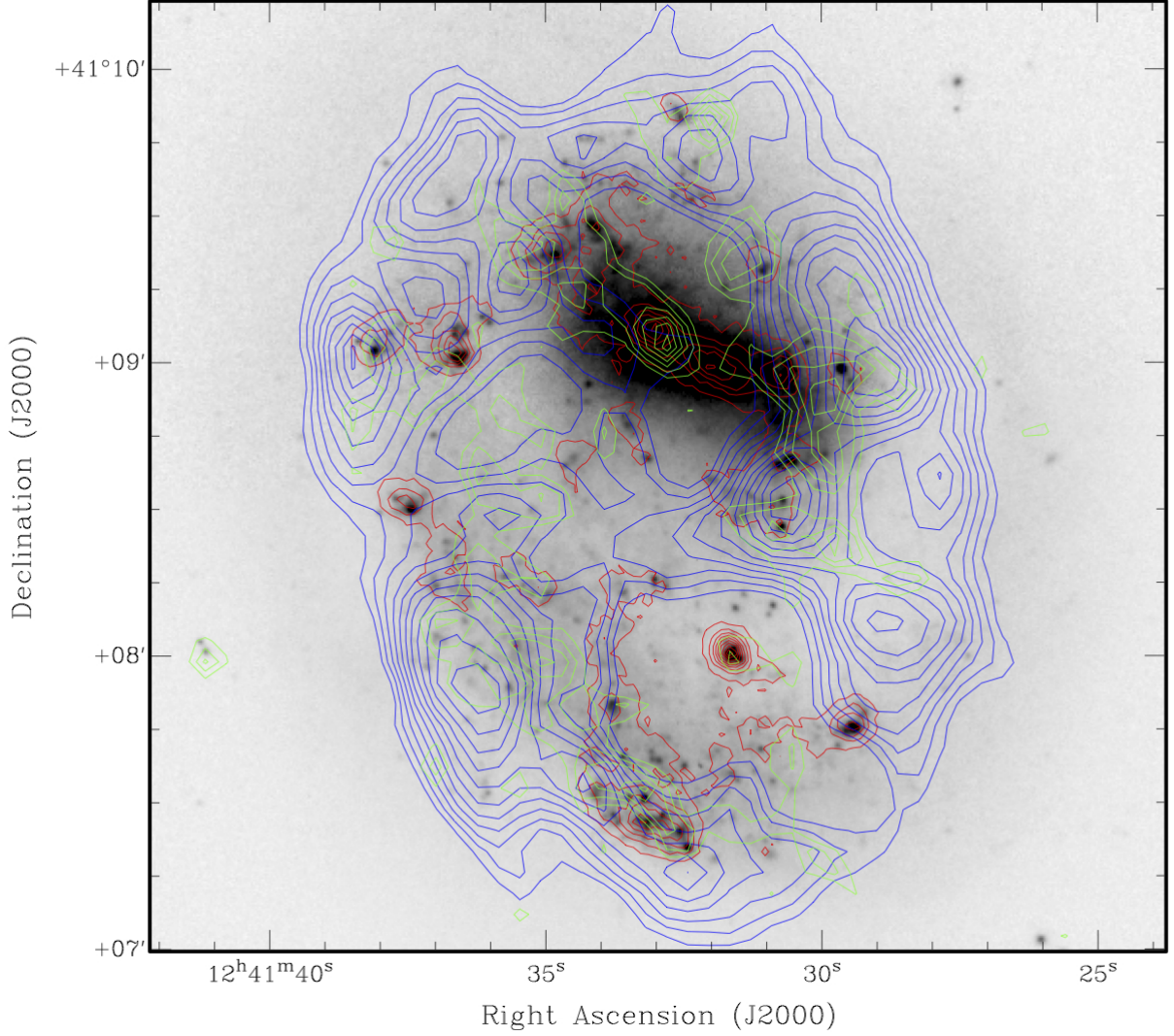


Fig. 10.— SDSS optical image of NGC 4618 overlaid with NUV (red), robust 5 H I column density (blue) and 1.4 GHz continuum (green) contours. The H I contours correspond to every 5% increase in density ranging from  $9.63 \text{ M}_{\odot} \text{pc}^{-2}$  to  $21.4 \text{ M}_{\odot} \text{pc}^{-2}$ . UV contours represent increases of  $3.9 \times 10^{-2} \mu\text{Jy}$ , or 10% increments in intensity. The continuum contours range from 72 to 131  $\text{mJy B}^{-1}$  in increments of 17  $\text{mJy B}^{-1}$ . These fluxes correspond to a range in star formation rate from  $2.39 \times 10^{-5}$  to  $4.35 \times 10^{-5} \text{ M}_{\odot} \text{yr}^{-1} \text{kpc}^{-2}$  with each contour level representing a  $5.64 \times 10^{-6} \text{ M}_{\odot} \text{yr}^{-1} \text{kpc}^{-2}$  change. There exists an anti-correlation between the location of the H I holes and peaks in the UV. The strong stellar bar is shown to also have extensive UV and 1.4 GHz emission associated with it.

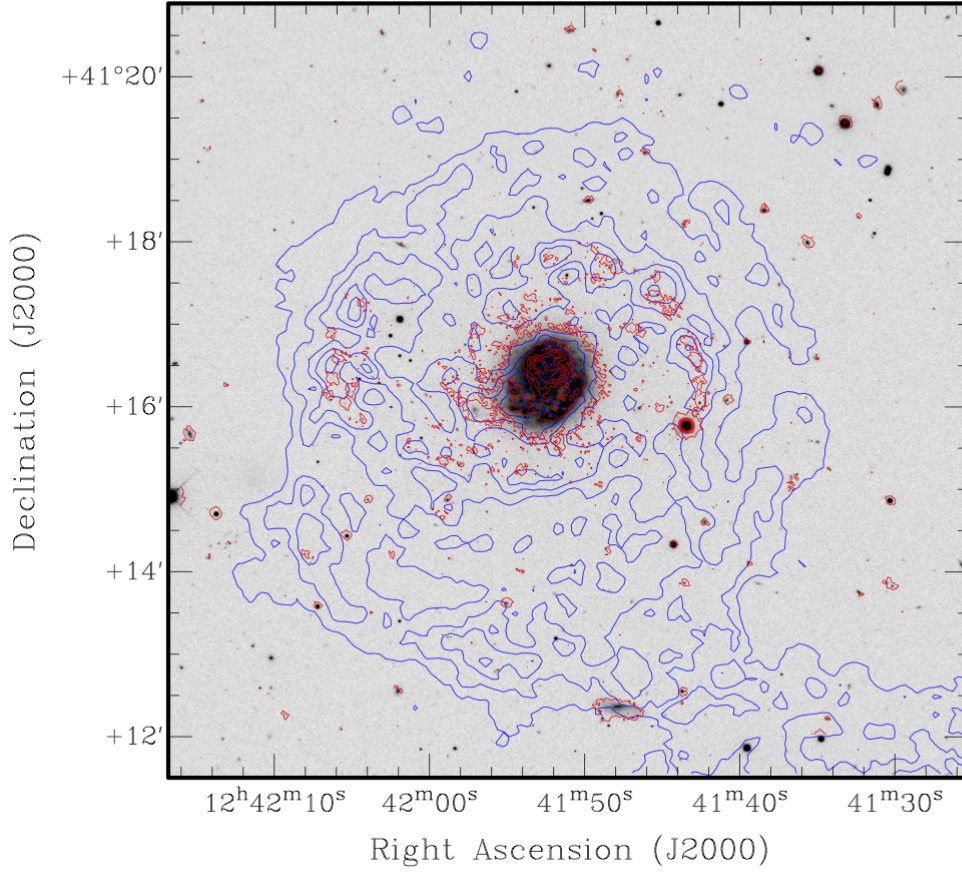


Fig. 11.— SDSS optical r-band image of NGC 4625 with *GALEX* NUV (red) and H I column density (blue). NUV contours correspond to increments of  $.048 \mu\text{Jy}$  spanning  $9.54 \times 10^{-3}$  to  $0.248 \mu\text{Jy}$ . H I contours map densities of  $1.1$  to  $6.42 \text{ M}_{\odot} \text{pc}^{-2}$  with increments of  $1.1 \text{ M}_{\odot} \text{pc}^{-2}$ . It is worth noting a bright area of UV emission ( $12^{\text{h}}41^{\text{m}}47^{\text{s}}$ ,  $+41^{\circ}12'22''.2$ ) south of NGC 4625 that is measured as having too low a H I density for star formation. Upon further investigation, it was found that the UV source originates from galaxy J124147.76+411222.2 at a redshift of  $z=0.0247$  as identified in the Sloan Digital Sky Survey archive. Radio continuum emission from this galaxy could be seen in our data cube before the continuum was subtracted in the cleaning process.



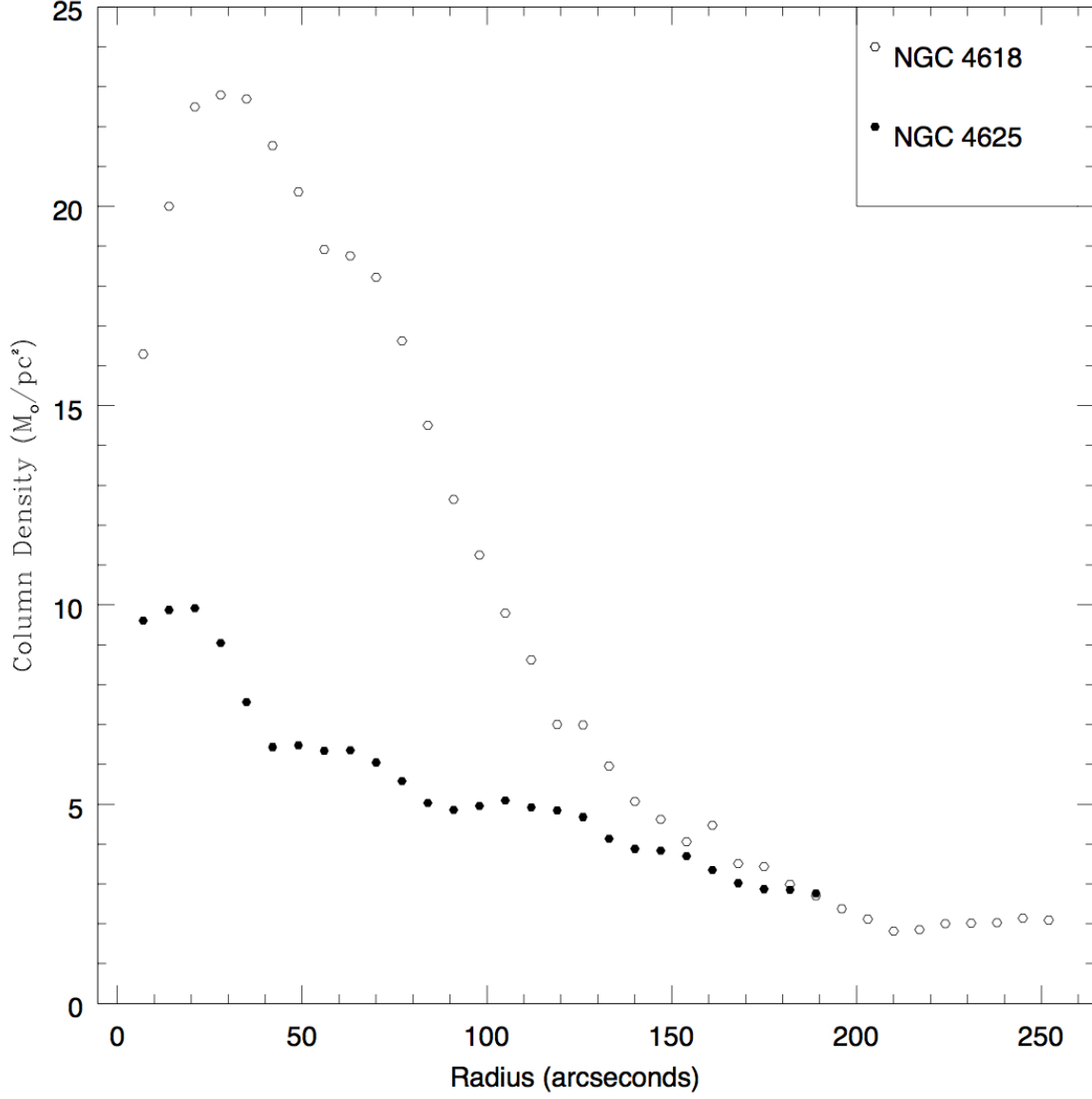


Fig. 12.— Radial plots of H I surface densities for both NGC 4618 and NGC 4625. Analysis is carried out to a radius equivalent to that of the rotation curve analysis with  $7''$  increments. The peak densities in both galaxies occurs within the core of each disk.



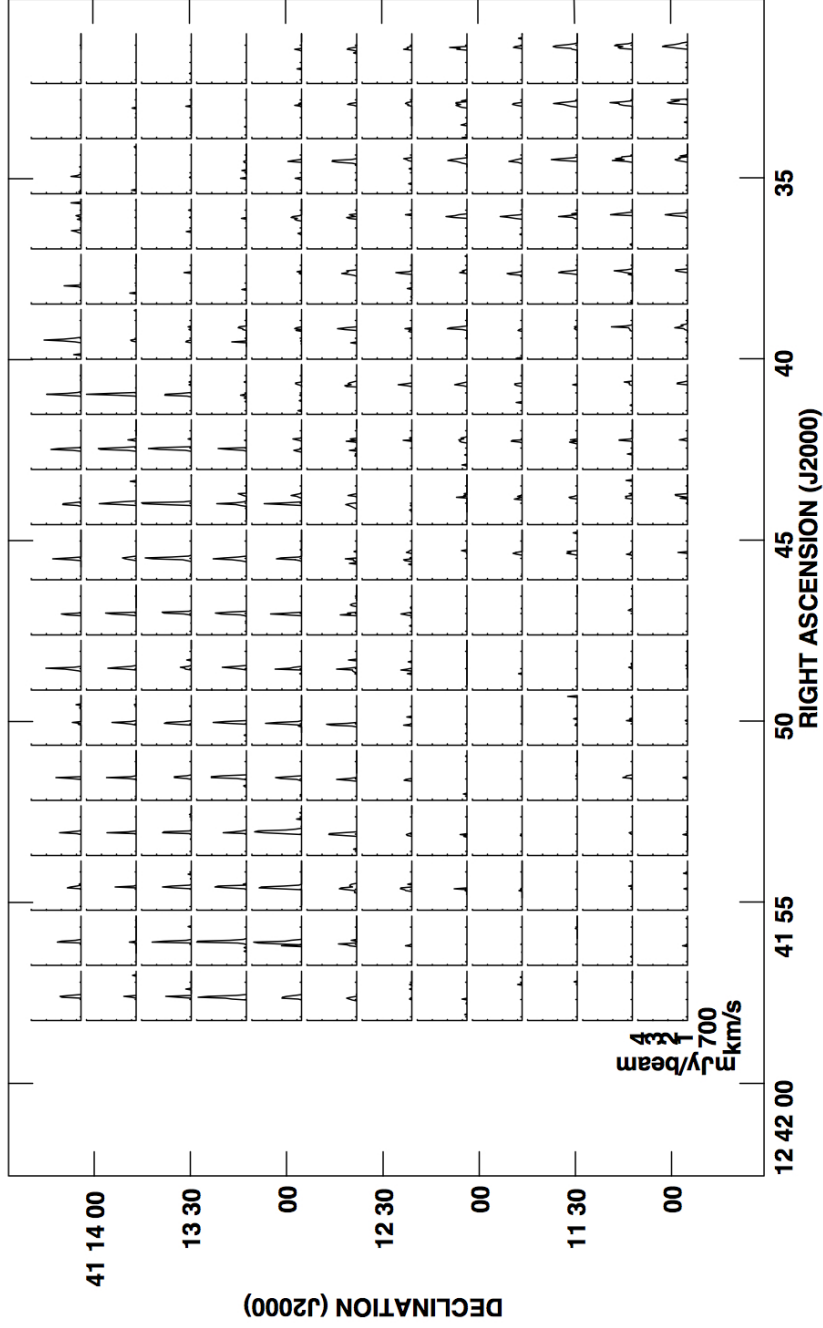


Fig. 13.— Line profiles of the H I gas corresponding to the area that is visually suggestive of an interaction. Each box shows the line profile for the gas in an area equivalent to one beam on the galaxy. The southwestern part of NGC 4625 appears in the upper left of the image, while the northeastern part of NGC 4618 appears in the lower right. The region of apparent overlap is in the middle of the image. This is the same region for which we see very high velocity dispersions in Figure 4. At first glance this would be suggestive of an interaction between the two galaxies. This image, however, shows that the apparently high velocity dispersions arise from the fact that there are two distinct kinematic components contributing to the overlap. Thus, the existence of double peaks in the RA range of  $12^h 41^m 40\text{--}47^s$  argues against an interaction.